Boiling and Condensation in Heat Transfer Equipment, Boston, ASME, 1987.

EXPERIMENTAL MEASUREMENTS OF CONDENSATION ON VERTICAL PLATES WITH ENHANCED FINS

M. A. Kedzierski and R. L. Webb
Department of Mechanical Engineering
The Pennsylvania State University
University Park, Pennsylvania

ABSTRACT

Fins were accurately machined on vertical plates with the electric discharge (EDM) process. Condensation heat transfer data for various fin shapes were used to experimentally demonstrate the importance of large curvature and curvature gradients for surface-tension drainage. A semi-experimental method was developed to verify the surface-tension condensation theories of Gregorig and Adamek. The semi-experimental method was the first used to isolate condensation regions of a finned surface. Experimental and theoretical analysis of combined surface-tension and gravity drainge condensation in channels are presented.

NOMENCLATURE

A	total surface area of plate, m^2
A_p	projected area of condensing surface (WL), m^2
b	y^*-intercept of Wilson Plot
CR	abreviation for constant radius
e	overall fin height, m
E_Q	% diff. between Q from temp.-grad. and Q from cond.-catch method,
fpm	fins per meter, m^{-1}
h	condensation heat transfer coefficient based on A, W/m^2-K
H	height of plate, 50.8 mm
h_p	condensation heat transfer coefficient based on A_p, W/m^2-K
k_m	thermal conductivity of condensing plate, W/m-K
L	total length of plate in z-direction, 101.6 mm
L_{ht}	heat transfer length of channel side, m
m	logarithmic slope of h versus ΔT plot,
m^*	slope of Wilson Plot, 1/m
$\dot{m}_e$	total condensate flow rate per channel, kg/s
n	logarithmic slope of h_s versus ΔT plot,
N_c	number of drainage channels in test plate,
N_f	number of fins on test plate (N_c - 1),
Q	measured heat load of plate, W
s	coordinate along fin shape, m
t_r	thickness of fin-root (at base of fin), m
T_{SAT}	saturation temperature of vapor, K
T_w	temperature of condensing surface, K
T_{Sp}	T_{SAT} from P_v measurement, K
T_{St}	T_{SAT} from thermocouple, K
U	overall heat transfer coefficient, W/m^2-K
U_∞	vapor velocity past test plate, m/s
X	functional dependance of Q_s, 1/m
x^*	coordinate along L_s, ordinate at $\delta = \delta_o$(m)

Greek symbols

Γ	mass flow rate per unit width, kg/s m
δ_b	thickness of condensate film on L_b, m
ΔT	$(T_{SAT} - T_w)$, K
κ	curvature, m^{-1}
λ	latent heat of vaporization of condensate, J/Kg
$\Delta\rho$	$(\rho - \rho_v)$, kg/m^3
σ	surface-tension of condensate, N/m
$\sigma\%$	standard deviation of E_Q,
τ_v^*	dimensionless interfacial vapor shear stress,
τ_v	interfacial vapor shear stress, N/m^2

Subscripts

b	channel bottom
f	convex fin surface
s	channel side

INTRODUCTION

Enhanced condensing geometries have been used since the late 1940's, when horizontal integral-finned tubes were introduced. Beatty and Katz [1], proposed that the heat transfer phenomenon was governed by gravity drained film condensation from the fin surface. Webb, Keswani, and Rudy [2] have shown that a significant contribution to the heat transfer enhancement of the horizontal integral-fin tubes is due to surface-tension forces that drain the condensate film from the fins. The contribution of Webb et al. [2] proved the concept that only specially shaped fins like those of Gregorig [3] can exhibit surface-tension drainage forces. Gregorig's 1954 publication on vertical flutted tubes was the

first to propose surface-tension as an enhancement for condensation. In 1980, Adamek [4] extended the theory of Gregorig by introducing a family of fin geometries of different aspect ratios that exhibit surface-tension drainage. Therefore, the information provided by the above authors suggest that the integral-fin geometry used in horizontal tubes need not be of the special shapes proposed by Gregorig or Adamek to exhibit surface-tension enhancement.

Laplace [5] has shown that, if a liquid-vapor interface is curved, a pressure difference across the interface must be present to establish mechanical equilibrium. The equilibrium condition is described by the curvature of the liquid vapor interface (κ) as:

$$P - P_v = \sigma (\kappa_1 - \kappa_2) \quad (1)$$

When applied to film condensation, the pressure difference is between the film and its saturated vapor.

The liquid-vapor interface of a condensate film must have a curvature decrease along the fin length in order to exhibit surface-tension drainage. The curvature decrease of the interface induces a pressure decrease within the film. This pressure variation is known as the surface-tension pressure gradient. The expression for the surface-tension pressure gradient is obtained by differentiating Eq. 1 with respect to the fin arc length (s), i.e.:

$$dP/ds = \sigma \, d\kappa/ds \quad (2)$$

EXPERIMENTAL PROGRAM

The purpose of this paper is to provide data for surface-tension drained condensation of various fin geometries on vertical plates. Fig. 1 illustrates surface-tension drained condensation on a vertical finned plate. The film is of thickness δ. The figure also distinguishes the convex fin region from the channel region. The convex fin region (double cross hatch) lies within the arc length S_m, and the channel region lies within the length L_s. S_m is the length over which the fin curvature changes. The coordinate system of the fin is also shown in Fig. 1. The curvature in the direction of gravity (z-axis) is zero. Hence the curvature of fin varies only with its arc length s. The curvature change produces a surface-tension pressure gradient that drives the condensate in the s-direction. In otherwords, the curvature reduction along Sm causes a pressure drop along Sm. There is an additional pressure drop due to the concave condensate radius in the channel corner. The condensate is pulled along Sm, L_s and into the channel corner. The condensate is then drained by gravity in the downward z-direction. The postulated streamlines of this flow are also shown in Fig. 1.

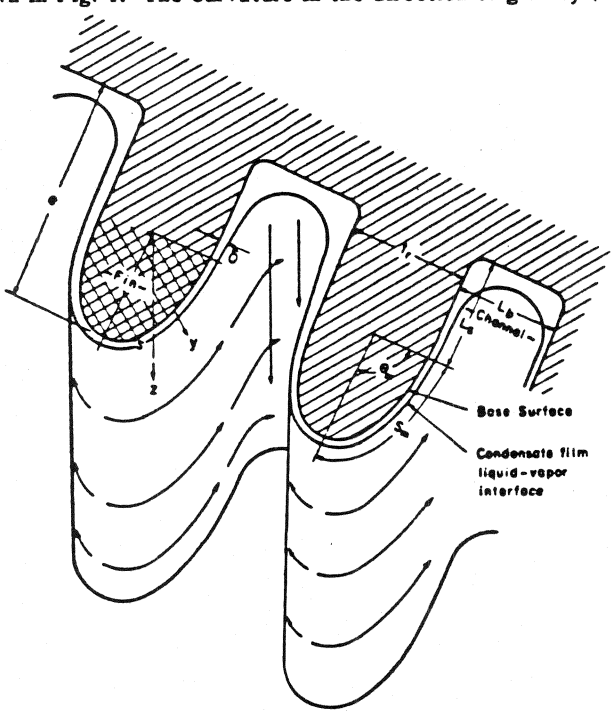

Fig. 1: Finned Surface with Film, Streamlines and Coordinate System

The data presented in this chapter are intended to permit validation of the analytical theories of Gregorig and Adamek [3,4]. No condensation heat transfer data exists for the optimum fin geometry as specified by Adamek [4]. There have been several condensation heat transfer tests of the Gregorig fin geometry since Gregorig's experiments in 1954. There are two limitations associated with the published data on the Gregorig fin geometries [3,6]. First, the fins were machined onto a vertical tube by tearing away the metal with a cutting tool. Gregorig gave the tolerance of his machining process as ±0.01 mm. The tolerance of the fins made by the electric discharge machining (EDM) process was ±0.003 mm. Second, the condensation on the Gregorig fin was not experimentally separated from the condensation that occurred in the channel. Also, the channels were not designed for adequate drainage. The thick film in the drainage channel would have disturbed the thin film of the fin. Therefore, the data could not be used to validate Gregorig's theory.

Gregorig's and Adamek's [3,4] analyses predict only the fin condensation on the arc length S_m. A semi-experimental method was developed to isolate the condensation that occurs on the fin from the condensation in the channel. Condensation heat transfer data for vertical plates having fin geometries used on horizontal tubes are presented for comparison with the heat transfer data of the Gregorig geometry and Adamek's optimum fin geometry. Condensation heat transfer data for constant radius fins are also given.

The purpose of testing fins on vertical plates rather than on horizontal tubes was to eliminate the complications associated with condensate retention on horizontal tubes [7]. Condensate retention on the vertical plates tested here is insignificant compared to that on horizontal tubes. Also, radial conduction and variation of the gravity component with the fin are eliminated by testing on plates instead of tubes. Most importantly, high machining precision is possible with the EDM method. The roughness of the plates of the present work machined with the EDM process was measured. The roughness was 0.002 - 0.004 mm. Consequently, the precision of the EDM process was ±0.002 - ±0.004 mm. This process can be applied to only a flat surface. It is not possible to EDM special fin shapes onto a round tube with high precision.

Heat Transfer Test Sections

The EDM process permitted us to use 600 data points to describe each fin profile. The accuracy of the EDM process was at least an order-of-magnitude greater than a gear milling process. Also, the EDM process was repeatable; that is, each fin was exactly the same. This is contrary to a gear milling process where the gear erodes after each cut, thus altering the gear shape.

Table 1 gives the dimensions of the machined fin geometries. Table 2 shows the area ratios of the plates. The overall plate length (L) was 101.6 mm for all of the condensing plates. The plate width (W) was approximately 50 mm for each plate. The plate height (H) was 50.8 mm for all of the condensing plates.

Fig. 2 shows actual cross sections (drawn to scale) of the machined condensing surface for all of the finned plates tested. Drainage channels (dimension L_s) were added to all of the fin geometries except for the commercial surfaces (Fig. 2e, Fig. 2f).

Fig. 2a and Fig. 2b show the Gregorig and Adamek's

Table 1: Dimensions of Finned Plates

Test Plate	fpm	Fin Dimensions (mm) e	S_m	t_r	Trough Dimensions (mm) L_s	L_b
Greg #1	577	.554	.762	.716	.254	1.016
Greg #2	577	.554	.762	.716	.508	1.016
Greg #3	577	.554	.762	.716	.762	1.016
Admk #1	746	.703	.762	.325	.254	1.016
Admk #2	746	.703	.762	.325	.508	1.016
Admk #3	746	.703	.762	.325	.762	1.016
GEWA-T	663	1.20	2.12	1.14	N/A	N/A
Integral-Fin	748	1.52	1.84	.457	N/A	N/A
Const. Radius (0.4mm)	553	.397	.623	.794	.397	1.016
Const. Radius (0.8mm)	384	.794	1.25	1.59	.397	1.016

Table 2: Area Ratios of Finned Plates

Plate	A (mm^2)	A_f/A	A_s/A	A_b/A	A/A_p
Greg #1	9532.88	0.5	0.167	0.333	1.74
Greg #2	11132.89	0.43	0.29	0.29	2.03
Greg #3	12732.88	0.375	0.375	0.25	2.32
Admk #1	11406.43	0.5	0.167	0.333	2.23
Admk #2	13316.16	0.43	0.29	0.29	2.61
Admk #3	15226.81	0.375	0.375	0.333	2.98
GEWA-T	14070.00				2.75
Int.-F	15034.00				2.94
CR (0.4mm)	7978.64	0.41	0.26	0.33	1.49
CR (0.8mm)	8304.70	0.58	0.18	0.24	1.51
Flat Plt.	5483.86				1.00

optimum fin shape, respectively. The dimension L_s is the length of the channel side. The arc length defined by S_m is the fin surface. The value of L_s for the Gregorig #1, the Gregorig #2, and the Gregorig #3 plate is 0.254 mm, 0.508 mm, and 0.762 mm, respectively. The fin shape and the channel width (L_b) of the Gregorig plates remained unchanged. The channel side length (L_s) for the Adamek plates were varied in the same way as the Gregorig plates. The theories of Gregorig and Adamek predict only the condensation that occurs on the convex fin surface (S_m). In the present test method, the condensation that occurs on length S_m is separated from that on the flat sides (L_s). Hence, the condensation coefficient on S_m can be compared with the theoretical values.

Fig. 2c and Fig. 2d show the cross sections of constant radius (CR) plates #1 and #2, respectively. The channels of these plates (L_s, L_b) are identical, but the fin sizes are different. The constant radius plate #1, and #2 have a fin radius of 0.4 mm and 0.8 mm, respectively. The data from the constant radius plate are analyzed to provide channel heat transfer information by a method similar to that used to isolate the fin condensation on the Adamek and Gregorig plates.

Fig. 2e and Fig. 2f show the cross section of the GEWA-T [8] and the Integral-fin surfaces, respectively. The shapes shown are a close replica of the commercially available shapes [8]. The data from these plates will serve as a reference for all the plates tested.

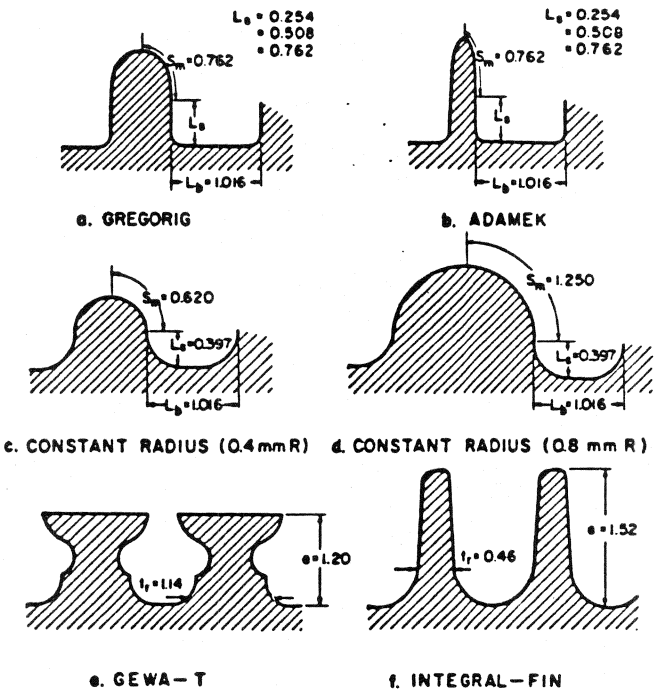

Fig. 2: Cross Sections of Condensing surfaces (all dimensions in mm)

Test Apparatus

Fig. 3 shows a schematic of the test apparatus. The test section was installed in a cell whose interior dimensions were 64 x 146 x 305 mm. The test chamber was supplied with saturated vapor by the boiler. The electric heated boiler had a maximum output of 22.5 KW. The boiler contained six immersion heaters, one which was controlled by a variable transformer to regulate the heat-supply boiler. Approximately 80% of the vapor produced by the boiler traveled past the test section and to a post condenser where it was condensed and returned to the boiler by natural circulation. The post condenser had approximately 10 m of 19 mm diameter 1024 fpm integral-fin tubes in six waterside passes. Equilibrium between the amount of vapor produced by the boiler and vapor condensed by the post condenser and the test section established the operating pressure of the apparatus. The condensing pressure was held at 1305 ±5 mm Hg. The pressure of the boiler, the post condenser, and two locations in the test chamber were measured with an absolute mercury manometer. The saturation temperature of the vapor was obtained from the measured pressure and the saturated property data of R-11. The power input to the boiler was measured by a wattmeter. A Fluke 2200B data logger was used to measure the voltage output of 16 thermocouples, 12 of which were in the condensing block. Two thermocouples were used to measure vapor temperature; one in the boiler and another in the post condenser. The vapor temperatures obtained from the thermocouples were used only as a check for the temperature deduced from the measured pressure and the saturation curve. The remaining thermocouples were located in the inlet and exit of the coolant water for the post condenser. The data logger had the capability to measure the sixteen temperatures consecutively within four seconds. A precision mercury thermometer (0.05C/graduation) was used to measure the vapor temperature of the test chamber. This temperature measurement was used only as a check for the saturation temperature obtained from the vapor pressure measurement. Two Hewlett-Packard™ model 2804A quartz thermometers were used to measure the temperature change

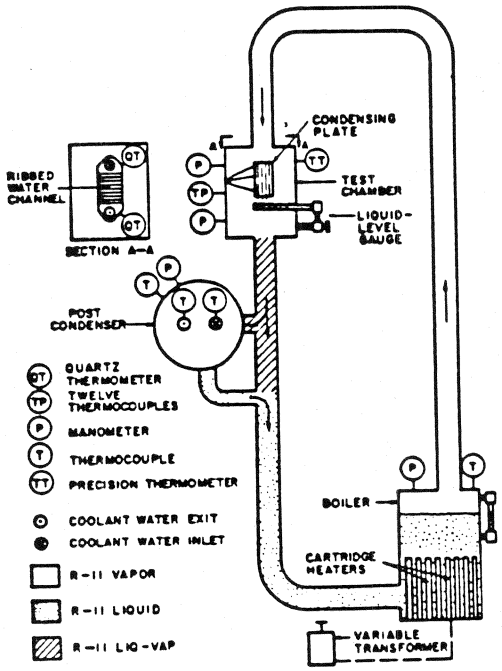

Fig. 3: Schematic of Condensation Test Apparatus

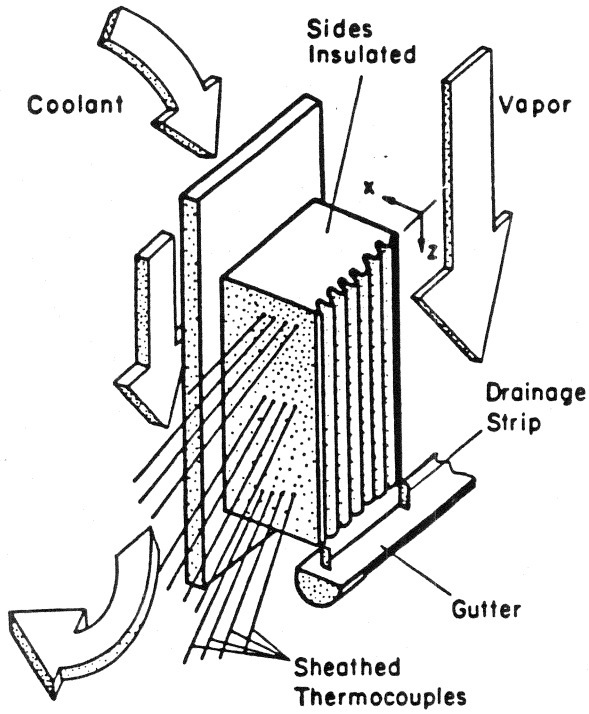

Fig. 4: Condensing Plate Instrumented For Data Acquisition

of the cooling water to the test plate. A weigh tank was used to measure the mass flow rate of the cooling water to the test chamber and to the post condenser. The light from a stroboscope was directed through a window in the test chamber to examine the condensate film for ripples or any other disturbances.

Test Procedure

Fig. 4 shows a test plate instrumented for data acquisition. The finned surface of the plate was exposed to saturated R-11 vapor. The back of the plate was cooled by high velocity water. The water flow was thoroughly mixed by ribs which were machined on the coolant channel. Twelve 0.51 mm diameter sheathed thermocouples were embedded 19 mm deep within the copper plate. The hole diameter was 0.53 mm. The thermocouples were spaced at three different positions in the z-direction of the plate. The four thermocouples at these positions were evenly spaced at 10 mm. The temperature profiles were used to determine the temperature gradient and the surface temperature at the fin-root for each z-position. The plates have such high thermal conductivity that the fin efficiency was always within the range 0.97-0.99. The four sides of the plate were insulated in order to produce one-dimensional conduction in the x-direction. Heat conduction along the thermocouples was minimized by their 19 mm deep insertion in the plate-side. A drainage strip at the end of the plate directed the condensate into the gutter which carried it to a liquid-level gauge. This gauge was used to measure the condensation rate on the plate.

The heat load of the plate was obtained by two independent methods. The first and more accurate was the temperature gradient method. The three sets of four thermocouples were used to obtain the temperature gradient (dT/dx) at the three axial positions. Fouriers's law, the known thermal conductivity of the metal (k_m), and its cross sectional area (A_p) were used to obtain the heat load (Q),

$$Q = k_m A_p \, dT/dx \qquad (3)$$

The second method used to obtain the heat load of the plate was the condensate catch method. The mass flow rate of the condensate drainage from the finned surface was determined by measuring the time required for the condensate to fill a known volume in the liquid-level gauge. The heat load of the plate was then obtained as the mass flow rate of the condensate multiplied by the latent heat of the saturated vapor, i.e.,

$$Q = \dot{m} \lambda \qquad (4)$$

The error in the heat load data was due to errors in the measurement of the vapor pressure, measurements of temperatures, and measurements of flow rates. The maximum possible error in the heat load measurement (for 99.7% confidence) was ±5% of the measurement. The error in the heat transfer coefficient may have been as large as ±10% (maximum possible error), but probably was not larger than ±6.4% (99.7% confidence).

Considerable effort was made to ensure that the apparatus was free of noncondensible gases before testing. First, the entire apparatus was evacuated and then filled with R-11 vapor to a pressure above atmospheric. Then the system was checked for leaks with a Halogen leak detector. Once all the leaks were found and sealed, the system was evacuated again. The vacuum pump continued to operate five or more hours after the manometer indicated that the system pressure was 0 mm Hg. The boiler was then filled with R-11 liquid while the vacuum pump was left running for a short time during filling. Further purging was done by generating vapor and operating the post condenser. The post condenser was then vented to the atmosphere to remove any noncondensibles. Finally, the post condenser was always operated during testing. This ensured that if any noncondensibles remained, they would have been carried to the post condenser.

There were two checks for noncondensibles. The first check was to compare the saturation temperature obtain from the measured pressure and the measured saturation temperature. If the two temperatures always agree within a small system error (constant error), some confidence can be

given to negligible effect of noncondensibles. The systematic temperature error was approximately 0.2 K. Another method used to check for the effect of noncondensibles was to take data a few days apart. It was unlikely that the same amount of noncondensibles would be present in the apparatus on the two different days since air will tend to leak out due to a system pressure above ambient. If the data were repeatable then the effect of noncondensibles was negligible.

The actual recording of data was done when steady state was attained. Steady state was achieved only after the system pressure remained within 1305 ±5 mm Hg and the thermocouple outputs remained within ±0.002 mV of the steady state value for at least a 20 minute period. The stroboscope was always used to check the condensate surface for ripples before recording each data point.

The test procedure was qualified by testing a vertical flat plate and comparing the results to the solution of Rohsenow, Webber and Ling [9] for condensation on a vertical flat plate under the influence of vapor shear. Although their solution is for constant interfacial shear, accurate results can be obtained for flows with small Froude numbers ($Fr = U_\infty/(gL)$). For this type of flow, vapor shear is negligible compared to the drainage force of gravity. The average Froude number for the end of the plate deduced from the flat plate data was 0.07. Jacobs [10] has shown that for Fr (evaluated at L) equal to or less than 1, the error in the heat transfer introduced by the constant vapor shear assumption is negligible for more than 90% of the plate length. Since the Fr for the data is 0.07, the Rohsenow et al. solution accurately represents the heat transfer conditions of the flat plate data for essentially the entire plate length.

Fig. 5 shows the dimensionless heat transfer coefficient versus the film Reynolds number for different values of vapor shear at the liquid-vapor interface. The solution of Rohsenow et al. was plotted along with the present data. The agreement between the data and the model was within ±10% for all of data. This agreement established confidence in the test procedure and the data acquisition method.

EXPERIMENTAL RESULTS

Fig. 6 and Fig. 7 present data taken for the ten different finned plates. The figures are plots of the condensation heat transfer coefficient (based on the projected area of the finned plate) versus the temperature difference ($T_{SAT} - T_w$). Fig. 6 shows the heat transfer data for the six Gregorig and Adamek plates. Fig. 7 shows the heat transfer data for the GEWA-T, Integral-fin and the constant radius plates.

Table 3 shows the statistical evaluation of the heat transfer data for all of the plates. The first two columns contain the slope (m) and the standard deviation of the slope (σ_m) for the data given in Fig. 6 and Fig. 7. The m is the exponent for the slope of the h versus ΔT relationship, i.e.:

$$h = C_h (T_{SAT} - T_w)^m \qquad (5)$$

The theoretical m for laminar filmwise condensation is -0.25. The third column of Table 3 contains the percent difference between the heat load measurement obtained from the temperature-gradient data acquisition method and the condensate-catch data acquisition method. The agreement between the two methods was shown to be within ±6% for all of the data except for the Adamek #3 plate. Visual inspection of the condensation showed that a major fraction of the condensate of the Adamek #3 plate was not directed into the gutter. A faulty installation of the drainage strip caused the misdirection of the condensate. Condensate drainage for all other test plates was successfully directed into the gutter.

The fourth column of Table 3 shows the standard deviation of the difference between the two data acquisition methods ($\sigma_{\%}$) was small. The fifth column shows the agreement between the saturation temperature obtained from the vapor pressure measurement and that obtained from the

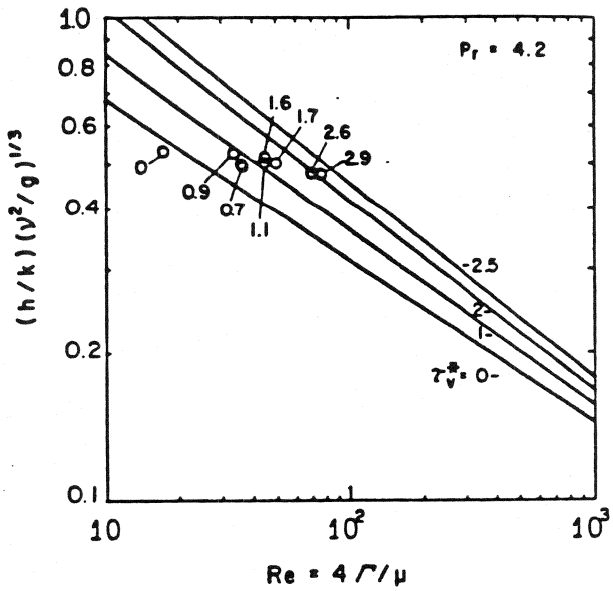

Fig. 5: Vertical Flat Plate Condensation Measurements

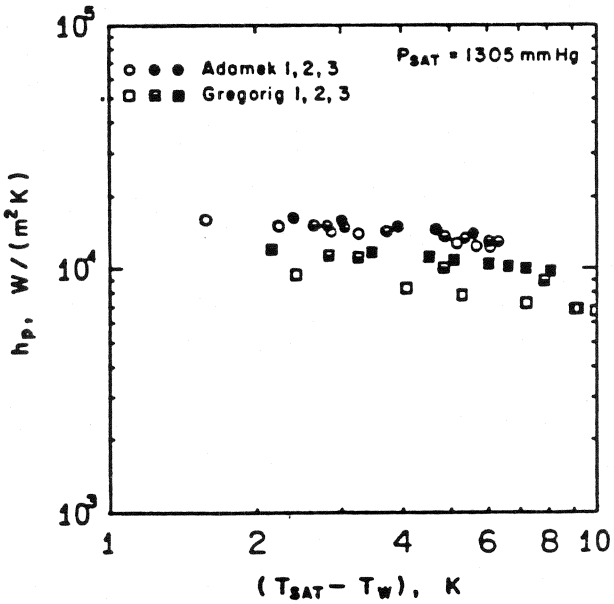

Fig. 6: Condensation Heat Transfer For Gregorig and Adamek Finned Plates (R-11)

thermocouple. The temperature obtained from the thermocouple was approximately 0.2 K below that obtained from the pressure measurement. The difference was shown to be relatively constant; indicating that the difference was a systematic error, not an error due to noncondensibles.

The sixth column indicates the presence or absence of ripples on the condensate film of the test plate. The constant radius (0.4 mm) plate was the only plate observed to have ripples. The ripples were present approximately 30 mm up from the drainage strip and only in the channels. No ripples were visible on the fin surfaces. The wavelength of the ripples was approximately 1.0 mm. They were viewed at a stroboscope setting of 2300 rev/min. The percentage of the channel length (L) that had ripples increased as the the film Reynolds Number ($Re = 4\Gamma/\mu$) increased. For example, for Re = 141 the ripples were present 32 mm up from the drainage

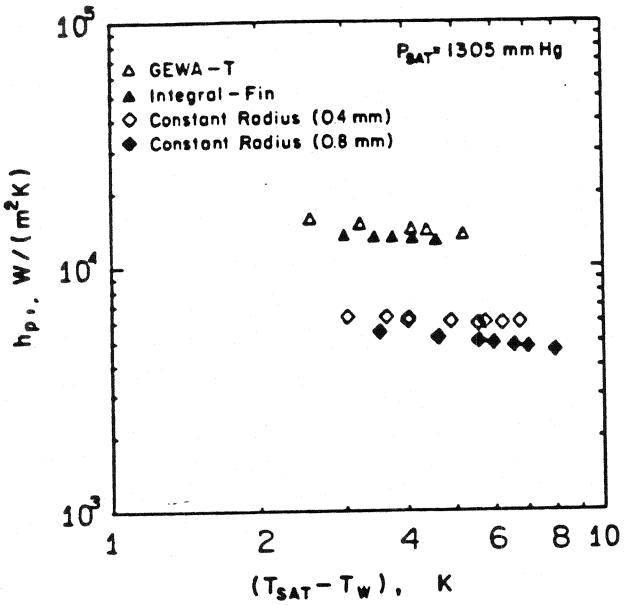

Fig. 7: Condensation Heat Transfer For Finned Plates (R-11)

Table 3: Statistical Evaluation of Data

Test Plate	Slope of h vs ΔT	σ_m	E_0	σ_t	TSp-TSt (K)	Ripples?
Greg #1	-0.243	0.00177	4.76	2.3	0.27	No
Greg #2	-0.231	0.00726	3.36	1.92	0.25	No
Greg #3	-0.207	0.0039	1.675	1.14	0.21	No
Adak #1	-0.203	0.00262	0.971	0.76	0.23	No
Adak #2	-0.191	0.0031	5.2	2.79	0.25	No
Adak #3	-0.187	0.00713	27.8	13.5	0.22	No
GEWA-T	-0.202	0.00454	1.9	0.03	0.21	No
Integral-Fin	-0.114	0.0092	3.6	0.7	0.19	No
Const. Radius (0.4mm)	-0.149	0.0146	1.5	1.3	0.25	Yes
Const. Radius (0.8mm)	-0.248	0.005	0.7	0.8	0.24	No

strip. This is 31% of the total channel length of 101.6 mm. For Re = 237 the ripple were present 50 mm up from the drainage strip. Thus, the ripples were present for nearly 50% of the channel. Since the ripples were present only in the lower portion of the channel (near the drainage strip) and the influence of the ripples increased for the higher heat loads, the cause of the ripples was attributed to the large mass flow rate of condensate in the relatively small channels.

DISCUSSION OF DATA

Fig. 8 is a plot of the heat transfer coefficient based on the total plate surface area (h) versus θ_T/S_T. The θ_T is defined as the angle that the arc length S_T turns starting from the fin tip and ending at the center of the channel. The S_T is defined in Fig. 9.

Fig. 8 shows four lines that are drawn through data of similar fin shapes. These lines illustrate that for fins of similar characteristics, a higher heat transfer coefficient was associated with the larger values of θ_T/S_T. The parameter θ_T/S_T is equal to the average curvature of the fin ($\bar{\kappa}_b$):

$$\bar{\kappa}_b = (1/S_T)\int_0^{S_T} \kappa_b \, ds = \theta_T/S_T \qquad (6)$$

where κ_b is the local curvature of the fin surface. Equation 6 shows that a small arc length rotated through a large angle gives a large curvature.

The curvature and its rate of change dictate the drainage force of the film. At the fin tip, a large curvature (small radius) sustains a film pressure which is larger than the saturation pressure of the surrounding vapor. The film pressure at the tip can be increased by decreasing the radius of the fin tip (r_o), that is, by increasing its curvature. The film pressure decreases to the saturation pressure as the arc length turns ninety degrees (at $s = S_m$, $\kappa_b = 0$). The rate of pressure decrease, the pressure gradient (dP/ds), is governed by the decrease of curvature along the arc length s, i.e.,

$$dP/ds \sim \sigma \, d\kappa_b/ds \qquad (7)$$

Equation 7 predicts a large drainage force for a fin with a large curvature gradient. In summary, fins with large fin tip curvatures (κ_o) and large curvature gradients ($d\kappa_b/ds$) will have large condensation heat transfer coefficients.

Equation 7 implies that a fin with constant curvature would have a zero pressure gradient. For this reason straight sided shapes and constant radius shapes have a relatively low

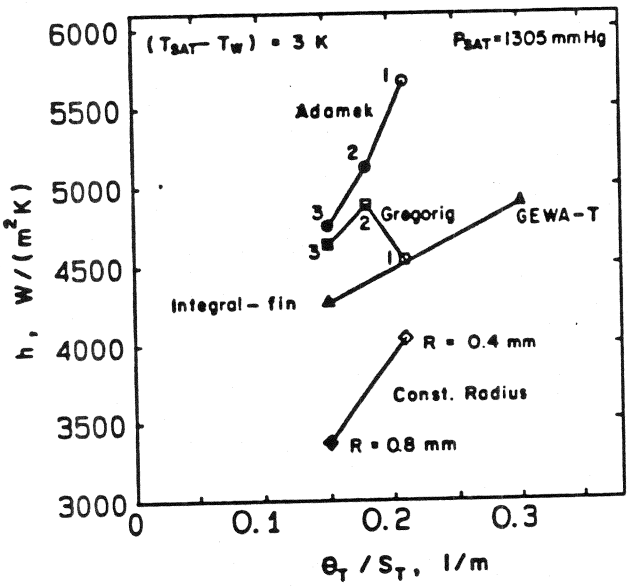

Fig. 8: Effect of Fin Curvature on the Composite Heat Transfer Coefficient (R-11)

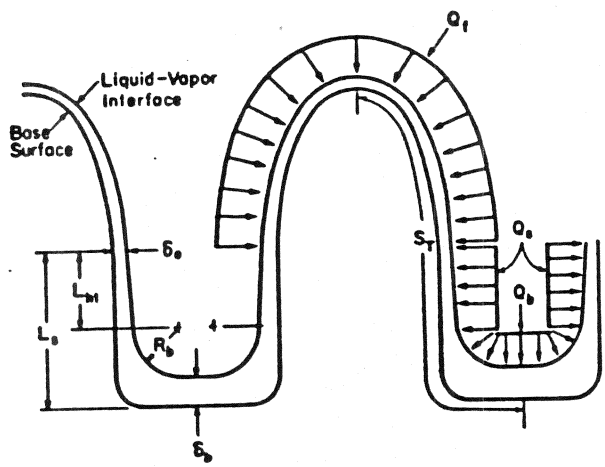

Fig. 9: Schematic of Heat Transfer Regions and Dimensions for Model

heat transfer enhancement. The present surfaces have straight drainage sides joined to the convex profiles, as illustrated by Fig. 2a through Fig. 2d. Thus, the composite heat transfer coefficient (h) will be somewhat lower than the heat transfer coefficient for the convex surface (h_{cx}), e.g.,

$$h\, S_T = h_{cx} S_m + h_s L_s + h_b L_b \qquad (8)$$

where the following are illustrated on Fig. 2a and Fig. 2b:
S_m = length of convex profile measured from fin tip
L_s = length of channel side
L_b = length of channel base

The condensation data given in Fig. 8 for the Adamek plates shows that this group has the highest heat transfer coefficients. The fin tip radius of the Adamek plates is 0.07 mm, which was the smallest of all plates tested. The curvature gradient at the fin tip was calculated to be -5×10^{10} ($1/m^2$), which was the largest of all the plates tested. Hence, the high performance of the Adamek plate was due to both the small tip-radius and the large curvature gradient at the fin tip. The composite h decreases for the Adamek #2 and #3 surfaces because of the increasing contribution of the channel side (L_s) to the total condensation. The channel sides have zero curvature change, hence their contribution to the enhancement was small.

The condensation data shown in Fig. 8 for the constant radius plates (Fig. 2c and Fig. 2d) shows that this group has the lowest composite heat transfer coefficients. The h of the constant radius fins are smaller than the Adamek fins because the fin tip radius was approximately ten times larger, giving a substantially smaller pressure in the condensate film. The plate with the smallest heat transfer coefficient has a radius of 0.8 mm. The data for the constant radius plates shows that fins with smaller radius tend to have higher performance. This is shown by the fact that the the 0.4 mm fin radius plate has a 15% higher heat transfer coefficient than 0.8 mm radius plate.

The heat transfer coefficient of the GEWA-T was larger than that of the integral-fin because the average curvature of the GEWA-T fin was larger. Equation 6 predicts that the average curvature of the GEWA-T is twice as large as the curvature of the Integral-fin. Both of these plates have a fin arc length (S_T) of 2.1 mm. But the angle through which the arc length of the GEWA-T is turned is twice as large as that of the Integral-fin. Therefore, it was not surprising that the heat transfer coefficient of the GEWA-T was 7% larger (at $\Delta T = 5$) than the heat transfer coefficient of the Integral-fin.

Isolation of the fin condensation

A key purpose of the tests was to verify the theories of Gregorig and Adamek. These theories predict only the heat load of the fin (Q_f). The heat transfer on the convex profile Sm is defined as Q_f. The fin regions of the condensing plates are defined in Fig. 9. The total heat load of the plate (Q) is measured for a fixed condensing pressure. Therefore, to compare the data to the theory, the heat load on the fin (Q_f) must be separated from the total (Q).

The separation of Q_f from Q required a predictive theory for the heat transfer to the bottom (Q_b) and the sides (Q_s) of the channel. The derivation of the equation to predict Q_b is given in Appendix A, the result is:

$$Q_b = 4/3[\lambda\, g\rho\, \Delta\rho\, (L_b N_c)^4 (k\, \Delta T\, L)^3/(3\mu\, Q)]^{1/3} \qquad (9)$$

Q_b was typically only 5% of Q. A 100% error in Q_b would produce only a 5% error in $Q - Q_b$. Therefore, the value $Q - Q_b$ was known with confidence. The derivation of the equation to predict Q_s is given in Appendix B, the result is:

$$Q_s = m^* X \qquad (10)$$

$$= m^* L_{ht}{}^3 R_b{}^{[illegible]} \mu\, \Delta T\, R_b L_{ht}{}^2/(\lambda\sigma\, \Delta\rho) + \delta_o{}^4]^{5/4} - \delta_o{}^5]$$

The right side of Eq. 10 shows Q_s as a constant (m^*) multiplied by its functional dependence, $X\{R_b\}$.

A "Wilson plot" [11] type method was used to ensure that Q_f had a dominant dependance on experiment rather than theory. The results of this method rely only on the functional form (not the absolute magnitude) of the predictive equation for Q_s. In summary, the Wilson plot was the mechanism that was used to obtain Q_f and Q_s from experimental data.

The Wilson plot method was devised by Wilson [11] in 1915, to separate individual heat transfer resistances from the overall resistances of a steam condenser. This method is most commonly used to determine the external heat transfer coefficient of a tube with knowledge of experimental values for the internal convective heat transfer and the overall UA. The overall energy balance of the tube is arranged to fit the following form:

$$y^* = m^* X^* + b \qquad (11)$$

All of the variables of Eq. 11, $-y^*$, m^*, X^*, and b— are functions of the unknown wall temperature (T_w). The parameters y^* and X^*, are the overall resistance and the external resistance, respectively. The slope m and the y -intercept are constants for the internal convection and the external heat transfer, respectively. The solution procedure for m^* and b is iterative. A guess for T_w is made and values for y^* and X^* are calculated and then plotted. Repeated guesses for T_w are made until the slope of the plot has converged. Convergence is attained when the the standard deviation of the slope has become close to zero.

The above procedure was modified to determine Q_f from the Gregorig and Adamek condensing plate data presented here. The first step of the procedure was to define an energy balance. Fig. 9 illustrates the energy balance for the finned plates. A mathematical statement of Fig. 9 is:

$$Q = Q_f + Q_b + Q_s \qquad (12)$$

Eq. 12 written in the form of Eq. 11 becomes:

$$Q - Q_b = m^* X\{R_b\} + Q_f \qquad (13)$$

The unknowns of Eq. 13 are the slope (m^*), Q_f, and the radius of the condensate in the channel corner (R_b). Equation 13 can be written once for the three Gregorig plates and once for the three Adamek plates for a fixed temperature difference. A plot consisting of three points (one from each plate) is made of $Q - Q_b$ versus $X\{R_b\}$ for assumed values of R_b. The radius of the condensate in the channel corner (R_b) is iterated until it has converged and the standard deviation of $Q - Q_b$ is close to zero. At convergence of Eq. 13, the $Q - Q_b$ intercept is Q_f. Since the fin shapes are identical for the three Gregorig and the three Adamek plates, Q_f must be the constant for each plate at the same temperature difference.

Fig. 10 shows the results of the Wilson plot at $\Delta T = 5$ C for the Gregorig and Adamek plates. The values of Q_f obtained from the plot are within ±5% of both Gregorig's and Adamek's theory for ΔT within the range 3-7 K.

Once Q_f was found from the Wilson plot, Q_s was obtained from Eq. 12. Fig. 11 presents a graph of the channel side heat heat transfer coefficient (h_s) versus ΔT for all of the Gregorig and Adamek plates. The slopes (n) of the lines are given beside them. Notice that all but two of the slopes are larger than the slope predicted by Nusselt [12] (-0.25). The composite heat transfer coefficient can be represented by a weighted sum of the individual heat transfer coefficients, i.e.:

$$h = (A_f C_f + A_b C_b)\Delta T^{-0.25}/A + A_s C_s \Delta T^n/A \qquad (14)$$

$$= C_h\, \Delta T^m$$

where $h_f = C_f \Delta T^{-0.25}$, $h_b = C_b \Delta T^{-0.25}$ and $h_s = C_s \Delta T^n$. Equation 14 demonstrates that the slope (m) of the data given

in Fig. 6 and Fig. 7 must be larger than -0.25 if n is larger than -0.25. Since the exponent n is larger than -0.25 the exponents (m) given in Table 3 must be between -0.25 and n.

Table 3 shows that the plates with the larger A_s/A ratios (see Table 2) also have the larger m's. Those plates with the larger A_s/A ratios have a larger fraction of Q contributed by Q_s. This demonstrates the correlation between channel condensation and a larger exponential dependence (m) on the heat transfer. Notice that for the Integral-fin m = -0.114, indicating that this flow is predominantly governed by channel type condensation, which is dependent upon the magnitude of the radius of the condensate in the channel corner.

Fig. 11 shows that h_s for the Adamek plates are 1.5 to 2.6 times smaller than the h_s for the Gregorig plates. The initial film thickness entering the channels of the Gregorig plates is half as large as that of the Adamek plates. Consequently, the Gregorig channels have a smaller film thickness (δ) on the flat sides (L_s) than for the Adamek plates. Since $h_s = k/\delta$, the Gregorig channels, because of smaller δ, have larger values of h_s.

CONCLUSIONS

The data presented show that finned surfaces with large curvature and curvature gradients are necessary for large condensation heat transfer enhancement. Commercially available surfaces had performances that were comparable to the theoretically optimum shapes of Gregorig and Adamek [3,4].

This is the first study to verify the analytical surface-tension condensation theories of Gregorig and Adamek. The verification was possible for two reasons. First, the semi-experimental method for the isolation of fin heat transfer is the first method to separate the fin condensation from the channel condensation. The theories of Gregorig and Adamek predict only the fin condensation. Consequently, to compare data to prediction requires the measurement of the fin condensation. Previous studies were unable to isolate the fin condensation. Second, the condensing plates were made with the EDM process. The EDM process permitted the specification of the fin shapes with high accuracy and precision. It is important to be able to accurately specify the fin shape since the pressure profile of the film is dependant upon the fin shape. Previous condensation measurements were made on fins which were machined by a less accurate and less precise tool cutting process.

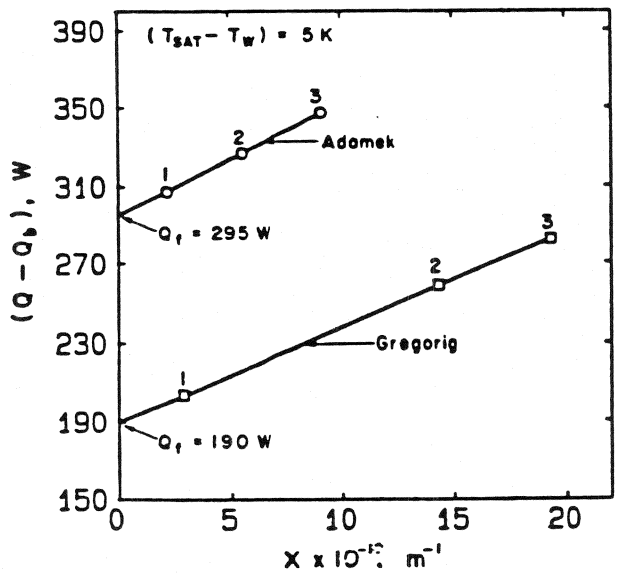

Fig. 10: Separation of Fin Condensation For Gregorig and Adamek Plates

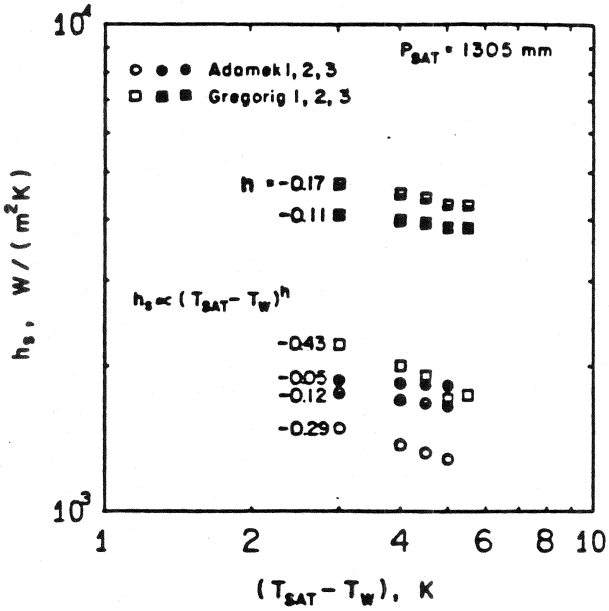

Fig. 11: Channel-Side Condensation (R-11)

The exponential dependence of channel condensation was found to differ from the theoretical exponent of -0.25. For most channels, the condensing exponent was found to be larger than -0.25, thus increasing the exponent of the composite plate heat transfer coefficient.

ACKNOWLEDGEMENTS

This research was supported by the National Science Foundation, Grant No. MEA-8306059. The Adamek, Gregorig and commercial condensing plates were manufactured by Wieland-Werke AG of West Germany. The constant radius plates were donated by the Aluminum Company of America.

REFERENCES

1. K. O. Beatty Jr., and D. L. Katz,"Condensation of Vapors on Outside of Finned Tubes,"Chemical Engineering Progress, Vol. 44, No. 1, 1948, pp. 55-70.

2. R. L. Webb, S. T. Keswani, and T. M. Rudy, "Investigation of Surface Tension and Gravity Effects in Film Condensation," Heat Trans. 1982, Vol. 5, Hemisphere Pub. Corp., Washington, D.C., pp. 175-180.

3. R. Gregorig, "Hautkondensation an feingewellten Oberflaechen bei Beruecksichtigung der Oberflaechenspannungen," Zeitschrift fuer angewandte Mathematik and Physik, Vol. V, 1954, pp. 36-49.

4. T. Adamek, "Bestimmung der Kondensationgroessen auf feingewellten Oberflaechen zur Auslegung optimaler Wandprofile," Waerme-und-Stoffuebertragung, Vol. 15, 1981, pp. 255-270.

5. P. S. Laplace, "Celestial Mechanics," Translated to English by N. Bowditch, Chelsea Publishing Company, Bronx, N.Y., 1966.

6. E. L. Lustenader, R. Richter, and F. J. Neugebauer, "The Use of Thin Films for Increasing Evaporation and Condensation Rates in Process Equipment", Jour. Heat Trans. Nov. 1959, p. 297-306.

7. Rudy, T. M., and Webb, R. L., "Condensate Retention on Horizontal Integral-Fin Tubes," Jour. Heat Trans. ,Vol. 107, No. 2, May 1985, pp. 361-368.

8. Anon., "Wieland Finned Tubes and Heat Exchangers," brochure #HE10-2, Wieland-Werke AG, Ulm, W. Germany, 1986.

9. W. M. Rohsenow, J. H. Webber, and A. T. Ling, "Effect of Vapor Velocity on Laminar and Turbulent-Film Condensation," Trans. ASME , Vol. 78, pp. 1637-1644.

10. H. R. Jacobs, "An Integral Treatment of Combined Body Force and Forced Convection in Laminar Film Condensation," Int. J. Heat and Mass Transfer, Vol. 9, pp. 637-648.

11. Wilson, E. E., Trans. ASME Vol. 37, p. 47-82, 1915.

12. W. Nusselt, "Die Oberflachenkondensation des Wasserdampfes," Z. Ver. Deut. Ing., 60, 541, 1916.

APPENDIX A: DERIVATION OF Q_b

The condensation that occurs on the bottom of the channel can be calculated from an analytical analysis similar to Nusselt's [12]. The average heat transfer coefficient of the channel bottom can be represented as:

$$h_b = (4/3)\, k/\delta_e \tag{15}$$

where δ_e is the film thickness at the end of the plate in the channel and k is the thermal conductivity of the condensate. The heat transferred to the channel bottom becomes:

$$Q_b = h_b\, L_b\, L\, \Delta T\, N_c \tag{16}$$

where L_b is the dimension of the channel from side to side, L is the vertical length of the channel, and N_c is the number of channels of the finned plate. The mass flow rate of the trough is represent as:

$$\dot{m} = g\rho\ \Delta\rho\ \delta_e\, L_b N_c/(3\mu) \tag{17}$$

Equation 17 represents the mass flow rate that comes out the channel end due to all of the condensation that occurs on the plate. Therefore, the mass flow rate can also be represented in terms of the total condensation as:

$$\dot{m} = Q/\lambda \tag{18}$$

By substituting Eq. 18 into 17 and solving for δ_e gives:

$$\delta_e = [3\mu Q/(\lambda g\, \rho\ \Delta\rho\ L_b N_c)]^{1/3} \tag{19}$$

Substitution of Eq. 19 into Equation 15 yields the relation for Q_b, i.e.,

$$Q_b = 4/3[\lambda\ g\rho\ \Delta\rho\ (L_b N_c)^4 (k\ \Delta T\ L)^3/(3\mu\ Q)]^{1/3} \tag{9}$$

APPENDIX B: DERIVATION OF Q_s

Fig. 9 shows the assumed shape of the liquid-vapor interface of the channel for the development of the expression for Q_s. The film thickness entering the channel (δ_o) is obtained from the theories of Gregorig and Adamek as the film thickness at the end of the fin. The condensate is assumed to gather in the channel corner to form a circular arc ($\pi/4$) of constant radius (R_b). The heat transfer that occurs along R_b is accounted for in the Q_b term. Thus, the heat transfer Q_s occurs only along the length L_{ht}:

$$L_{ht} = L_s - R_b - \delta_b \tag{20}$$

The pressure gradient from δ_o ($s = S_m$) to the intersection of R_b and L_{ht} is assumed to be constant, and represented by:

$$dP/ds = -\sigma/(R_b\, L_{ht}) \tag{7}$$

The governing differential equation comes from a Nusselt type analysis:

$$\frac{d\delta^4}{dx} = \frac{-4k\mu\Delta T}{(dP/ds)\ \lambda\ \Delta\rho} \tag{21}$$

The integration of Eq. 21 over L_{ht} yields:

$$\delta^4 = \frac{-4k\mu\Delta T\, x^*}{(dP/ds)\ \lambda\ \Delta\rho} + \delta_o^4 \tag{22}$$

Integrate Eq. 22 over L_{ht} to obtain the average film thickness (δ):

$$\delta = \frac{\lambda\sigma\ \Delta\rho}{5k\mu\ \Delta T\, R_b L_{ht}^2}\left\{\left(\frac{4k\mu\Delta R_b L_{ht}^2}{\lambda\sigma\ \Delta\rho} + \delta_o^4\right)^{5/4} - \delta_o^5\right\} \tag{23}$$

Q_s can be expressed as:

$$Q_s = A_s\, k\, \Delta T/\delta \tag{24}$$

The final expression for Q_s becomes after substitution of Eq. 23 into Eq. 24 is:

$$Q_s = \frac{L_{ht}^3\, R_b 10\, L\, N_f \mu (k\Delta T)^2/(\sigma\ \lambda\ \Delta\rho)}{\{[4k\ \mu\ \Delta T\, R_b L_{ht}^2/(\lambda\sigma\ \Delta\rho) + \delta_o^4]^{5/4} - \delta_o^5\}} \tag{10}$$

Equation 10 is sufficient for the Wilson plot method to find Q_f. The only unknown of Eq. 10 is R_b, and this was obtained from the iteration scheme of the Wilson plot method. But in order to ensure that the converged values for R_b were realistic, a separate theory for R_b was developed. The following is a development of an equation for R_b obtained from the momentum equation subjected to the assumed liquid-vapor shape and heat load (Q) constraints:

$$Q = \frac{4N_c\lambda\rho g[0.265\, R_b^2 + \delta_b L_b/2]^3}{3\,\nu[R_b + \delta_b + L_b/2]^2} \tag{25}$$

Equation 25 should be weakly dependent on R_b. In other words, R_b is fixed by the channel width (L_b) and not the heat load (Q). The surface-tension forces act to minimize the surface area of the condensate in the corner of the channel. Therefore, an increase in the heat load to the channel will work to increase to film thickness on the bottom of the channel (δ_b). However the magnitude of R_b will not increase. The affect of an increase in Q will only change the location R_b with reference to the bottom of the channel. Consequently, the derivative of Eq. 25 with respect to R_b is equal to zero: ($dQ/dR_b = 0$). The result can then be solved for R_b., i.e.,

$$R_b = 3/4\left\{\sqrt{\delta_b^2 + L_b^2/4 + 3.067\delta_b L_b} - [\delta_b + L_b/2]\right\} \tag{26}$$

The agreement between the value obtained from Eq. 26 and that from the Wilson plot method was always within ±10% for all ΔT's.